RSC Advances

PAPER

View Article Online
View Journal | View Issue

Cite this: RSC Adv., 2017, 7, 15293

Residual oxygen groups in nitrogen-doped graphene to enhance the capacitive performance†

Mengying Yu,[a] Bingqiao Xie,[a] Yang Yang,[a] Yong Zhang,[b] Ying Chen,*[a] Weiye Yu,[a] Shanshan Zhang,[a] Luhua Lu*[a] and Dong Liu[c]

Received 23rd December 2016
Accepted 3rd March 2017

DOI: 10.1039/c6ra28596a

rsc.li/rsc-advances

Nitrogen-doped graphene (NG) was obtained from a facile and eco-friendly hydrothermal reaction and used as electrode materials for supercapacitors. The textural and chemical properties could be easily tuned by adjusting the basicity of the reaction environment. As the basic reaction conditions became stronger, the sheets of NG tended to stack together, the content of residual oxygen groups increased, but the nitrogen content decreased, which affected the electrochemical performance. The NG synthesized under a weak basic environment shows great pseudocapacitance and the largest electrochemical performance in a 6 mol L^{-1} KOH aqueous electrolyte when measured in a three-electrode system, which can be attributed to its randomly distributed and loosely stacked structure and high amount of residual oxygen atoms (12.8 at%). Furthermore, it presented excellent cycling stability with a capacitance retention ratio of 92.86% at the current densities of 5 A g^{-1} after 10 000 charge–discharge cycles in two-electrode configuration, which kept stable after 5000 cycles. These results implied that the NG sheets obtained by this simple eco-friendly approach are suitable for high performance supercapacitor applications.

1. Introduction

With the increasing energy demand owing to global warming and the depletion of fossil fuels, great efforts have been made to exploit various energy-related devices and to improve their efficiency of conversion and storage.[1,2] Supercapacitors, also known as electrochemical capacitors, are different from traditional capacitors, combining the advantages of both conventional dielectric capacitors and rechargeable batteries and can transport high power within a very short period and store high energy.[3] As a new class of two-dimensional carbon nanostructure, graphene has attracted considerable interest in its potential applications in supercapacitor electrodes due to its outstanding theoretical physical and chemical properties, such as outstanding electrical conductivity, high mechanical flexibility, exceptional large specific surface area, and excellent structural stability.[4–6] It is announced that a theoretical capacitance value of up to 550 F g^{-1} can be expected with a fully utilization of entire theoretical specific surface area.[7,8] However, the defects produced in the manufacturing process and the high tendency for graphene sheets to restack caused by the strong π–π interactions between neighbouring sheets result in a much lower real value of specific capacitance than its intrinsic theoretical capacitance.[9,10]

Nitrogen-doping is considered to be an efficient way to improve the capacitive behavior of graphene based electrode because of the extra faradic redox reactions between the electrolyte ions and the heteroatoms-containing functional groups, as well as the improvement of surface wettability, and electronic conductivity.[11–13] So far, several process have been explored to introduce nitrogen atoms into graphene skeleton for high performance supercapacitors, such as the thermal annealing of graphene oxide (GO) with NH_3 in high temperature,[14] nitrogen plasma,[15] chemical vapor deposition (CVD) in the presence of NH_3,[16] arc-discharge of carbon electrodes.[17] These methods suffered from either low-yields, high-cost or rigorous conditions and complicated equipment. Hydrothermal and solvothermal reactions have been proposed as efficient and facile approaches to obtain nitrogen-doped graphene (NG) sheets for supercapacitors.[18–22] For example, Wang *et al.* obtained NG by treating GO with nine different amino acid with different acidities, while the highest specific capacitance was from NG obtained by DL-aspartic acid, which was around 290 F g^{-1} at 1 A g^{-1} with low surface nitrogen content (1.0%).[23] Xie *et al.* prepared NG using hydrazine hydrate as doping agent, the obtained 3–5 layers graphene exhibited 217 F g^{-1} at 1 A g^{-1}.[24] Sun *et al.* synthesized

[a]Engineering Research Center of Nano-Geomaterials of Ministry of Education, China University of Geosciences, Wuhan 388 Lumo RD, Wuhan 430074, China. E-mail: chenying@cug.edu.cn; lhlu@cug.edu.cn; Tel: +86-027-67884292

[b]School of Materials Science and Engineering, Hefei University of Technology, Hefei, 230009, China

[c]Key Laboratory of Mineralogy and Metallogeny/Guangdong Provincial Key Laboratory of Mineral Physics and Materials, Guangzhou Institute of Geochemistry, Chinese Academy of Sciences (CAS), Guangzhou 510640, China

† Electronic supplementary information (ESI) available. See DOI: 10.1039/c6ra28596a

NGs *via* a simple hydrothermal reaction of graphene oxide (GO) and urea, and as prepared NGs exhibits excellent capacitive behaviors (326 F g^{-1}, 0.2 A g^{-1}) as well as superior cycling stability.[25] As mentioned above, the synthesis of NG is generally processed in basic environment, in which reduction and doping processes proceed simultaneously. It is known that the supercapacitor performance of NG is not only concerned with nitrogen-doping level, but also with the types of the nitrogen species. To be specific, pyridine nitrogen and pyrrole nitrogen play key roles in enhancing the specific capacitance of NG due to their pseudo-capacitive contribution, while graphitic nitrogen contributes to the improvement of electrical conductivity.[26] Moreover, hydrothermal synthetic NG inevitably contained oxygen groups owing to the incomplete reduction of GO, of which the carbonyl species are deemed to be capable of providing pseudocapacitance.[27] Even though the capacitance of NG has been reinforced to a certain degree, there is still a great of interest to further improve the capacitive of NG by tuning nitrogen content and types, as well as utilizing electrochemical active oxygen components.

Herein, we demonstrated a facile and effective one-step hydrothermal reaction at weak basic environment to obtain NG with abundant pyridine nitrogen, pyrrole nitrogen and carbonyl groups under the assistance of ammonium phosphate ($(NH_4)_2HPO_4$). As a type of non-toxic, non-corrosive and eco-friendly amphoteric ammonium salt, $(NH_4)_2HPO_4$ can not only conduct reversible ionization and hydrolysis in solution to stabilize the pH value of reaction environment, but also produce ammonia by hydrolysis which can be an effective nitrogen doping agent. The NG obtained under weak basic environment exhibited outstanding capacitive behavior in terms of highly specific capacitance, good rate capability, and excellent cyclability when used as electrode materials for supercapacitors. The simple and versatile approach provided in this work is also helpful for the further enhancement of graphene-based supercapacitors.

2. Experimental section

2.1 Materials

Graphene oxide (GO) was bought from XF nano Co., Ltd. (China). Ammonium phosphate ($(NH_4)_2HPO_4$) and sodium hydroxide (NaOH) purchased from Tianjing Chemical Reagent Co., Ltd., were all of analytical grade with no further purification. All the aqueous solutions were prepared in deionized (DI) water.

2.2 Preparation of N-doped graphene

The GO (0.05 g) was dispersed in deionised water (DI) (70 mL) by ultrasonication for 30 min to make a GO aqueous dispersion. Then 1.0 g $(NH_4)_2HPO_4$ and 0.3 g NaOH was added to this GO solution with continuous stirring for 1 h. The pH value was controlled at a weak basic environment before the solution was sealed into a 80 mL Teflon autoclave. The autoclave was kept in an oven at 170 °C for 12 h. After natural cooling to room temperature, the pH value of the mixture was measured before it was washed several times with DI water to make the pH = 7 (see in Table S1†), and the as-prepared black product was allowed to dry by freeze-drying. The resultant powder was labelled as NG2. For comparison, the sample obtained in nearly neutral and strong basic environment named NG1 and NG3 were prepared under the same experimental parameters but changing the amount of NaOH into 0 g and 2.5 g. The pH values for NGs before and after the reaction data can be seen in Table S1.†

2.3 Material characterizations

The microstructure and surface morphology of the samples were investigated by scanning electron microscopy (SEM, Hitachi S4800) and transmission electron microscopy (TEM, JEM 1200EX). The phase structure of the samples was measured by power X-ray diffraction (XRD) experiment on a D8-FOCUS (Bruker, German) using a Cu target (λ = 0.154 nm). The Raman spectroscopy of NGs were recorded using a RENISHAW Raman microscope (INVIA) system. Thermogravimetric analysis (TGA) was conducted under nitrogen gas from room temperature to 800 °C at a heating rate of 10 °C min^{-1} using STA 409 PC (NETZSCH-Gerätebau GmbH). The chemical characteristics of NGs were analyzed by X-ray photoelectron spectroscopy (XPS) with MULT1LAB2000 using a 72 w Al Ka radiation.

2.4 Electrochemical measurements in a three-electrode system

Electrochemical measurements were performed on an electrochemical workstation (CHI 760E, Shanghai CH Instrument Company, China) which has a three-electrode experimental setup. The measurements were all carried out in a aqueous electrolyte containing 6 M KOH at room temperature. The working electrodes were fabricated from the mixture of NGs, acetylene black and poly(tetrafluoroethylene) (PTFE) with a NG : acetylene black : PTFE weight ratio of 80 : 10 : 10. Platinum foil electrode was used as counter electrode, and Hg/HgO electrode was utilized as the reference electrode. The mixture was coated onto nickel foam substrate (1 cm × 2 cm) and the obtained sample was pressed under a pressure of 8 MPa to fabricate electrodes followed by drying at 120 °C for 12 h. Cyclic voltammetry and galvanostatic charge/discharge tests were carried out at different scan rates and current densities in the potential range from −1.0 to 0 V. Electrochemical impedance spectroscopy (EIS) measurements were carried out by applying an AC voltage with 5 mV amplitude over a frequency range from 0.01 Hz to 100 kHz at the open circuit potential. The mass specific capacitance (C_{sp}) was calculated using the equation $C_{sp} = I\Delta t/m\Delta V$ based on galvanostatic charge/discharge test, where I means the constant discharge current (A), Δt is the running time from 0 V to −1 V, m is the mass of active material in each electrode, ΔV indicates the voltage change after a full discharge.

2.5 Electrochemical measurements in a two-electrode system

The two-electrode symmetric cell was conducted in a CR2016 coin-type cell, with a modified polypropylene separator between

the pellets and 6.0 M KOH as the aqueous electrolyte. The working electrodes were the pellets fabricated by coating the slurry on the nickel foam, which was the mixture of NG (80%), acetylene black (10%) and poly(tetrafluoroethylene) (10%). Before the measurement, the assembled coin cells were aged for 24 h to ensure good soakage of the electroactive material by the electrolyte. The Cyclic Voltammetry (CV) tests at different scan rates and galvanostatic charge/discharge tests at different current densities were carried out on an electrochemical workstation (CHI 760E). The long-term galvanostatic charge–discharge was evaluated with a LAND CT2001A (Wuhan, China) multichannel galvanostat in the potential range of −1–0 V at a current density of 5 A g^{-1} for over 10 000 cycles. The specific capacitance was calculated according to the following equation: $C_s = 2I\Delta t/m\Delta V$, where C_s (F g^{-1}), I (A), Δt (s), m (g), and ΔV (V) are the specific capacitance, the discharge current, the mass loading of NG on each electrode, the discharge time and the voltage window, respectively.

3. Results and discussions

3.1 Morphology and microstructures

SEM and TEM images were obtained to investigate the morphology and microstructure of the NGs materials. The SEM images (Fig. 1(a)–(c)) show the spatial morphology of the graphene samples. As shown in Fig. 1(a) and (b), it is clear that sample NG1 and NG2 which were synthesized under nearly neutral and weak alkaline environment preserve a randomly distributed, overlapped, and loosely stacked structure. Moreover, the sheets of NG1 seem to stack and coil into irregular channels, while that of NG2 tend to form an interconnected three-dimensional (3D) porous network structure like foam or a sponge. When the pH value of environment was up to 13.9, graphene sheets tended to stack together to form a bulk structure, as shown in Fig. 1(c). It clearly demonstrates that the pH value of the reaction environment has a significant effect on the NGs morphology. In order to further confirm the morphological features of nitrogen doped graphene, TEM analyses were carried out and the results were presented in Fig. 1(d)–(f). High transparent sheets with some visible wrinkles were observed in Fig. 1(d) and (e) since NG1 and NG2 were consisted of a few layers. In contrast, the sheets of NG3 were much thicker, which agrees with the results of SEM. It is known that, GO sheets are negatively charged in aqueous solution due to the ionization of the carboxyl and hydroxyl groups, and those electronegative groups cannot be fully reduced through hydrothermal treatment, resulting in negatively charged graphene sheets.[28] The different morphology of NGs could be attributed to the different electrostatic interactions caused by the reaction environment, this will be further discussed below.

3.2 XRD, Raman and TGA

The XRD patterns of NGs are shown in Fig. 2(a). The basal reflection peak of GO, which is at 11.8° as shown in the inset picture, disappeared in the XRD pattern of the NGs due to the exfoliation of graphene sheets during the hydrothermal process.[24] The appearance of a broad band centered at 25.5° is an indication of the formation of multiple layers of graphene.[26] The peak intensity for the NG1 sample was weaker than the other two indicating decreased restacking tendency in strong alkaline environment.[29]

Explicit evidence of N doping in the graphene network can be obtained by the Raman spectra analysis. Generally the intensity ratio of the D-band to the G-band (I_D/I_G) is used to estimate the defect lattices and degree of disorders in graphene.[30] The introduction of nitrogen atoms and the residue of oxygen atoms can distort original crystal lattice of carbon materials, and the increase of the defects can result in higher intensity of D band.[31] As shown in Fig. 2(b), I_D/I_G ratios of NGs increased slightly with the pH value, revealing strong base environment would affect the restoration of carbon network structure, which can be attributed to the increasing oxygen content in stronger basic environment (the corresponding data is shown below).

TGA were used to investigate the thermal properties of GO and NGs, as shown in Fig. 2(c). A slight weight loss of GO and NGs occurred below 100 °C was due to the release of physically

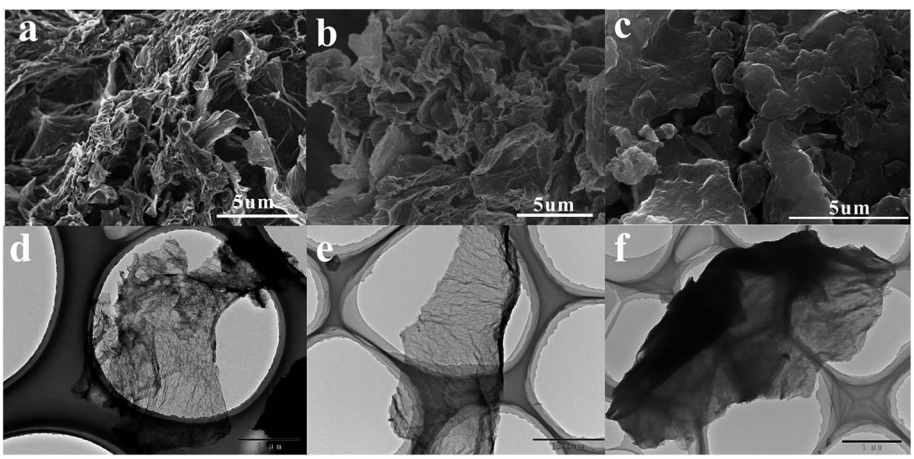

Fig. 1 SEM and TEM images of NG1 (a and d), NG2 (b and e) and NG3 (c and f).

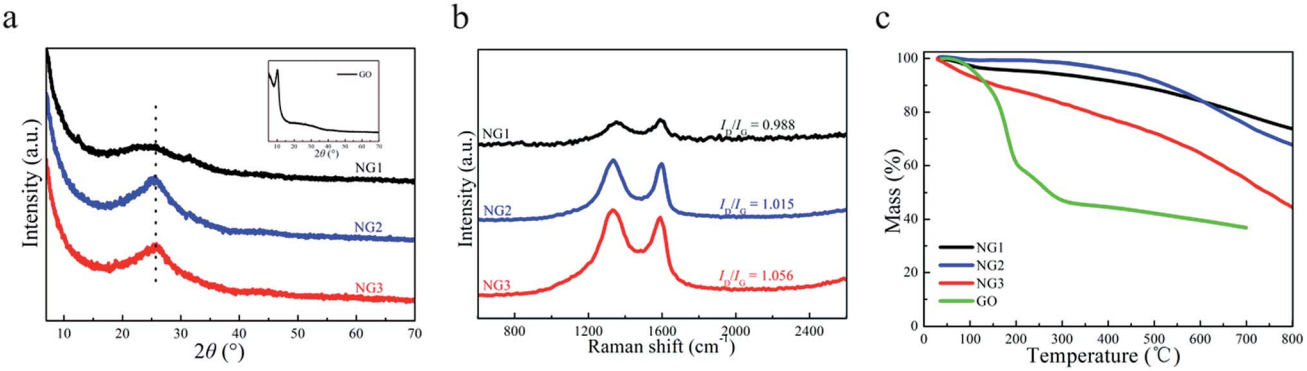

Fig. 2 XRD patterns (a), Raman spectra (b) and TGA curves (c) of NG1, NG2 and NG3.

adsorbed water.[32–34] As for GO, the major mass loss was recorded in the temperature range of 100–300 °C, which could be attributed to the decomposition of some oxygen functional groups such as –OH, –COOH and –C–O–C–.[32–34] Further weight loss at higher temperatures could be ascribed to the decomposition of the carbon skeleton and the remaining stable oxygenic functional groups (such as esters, *etc.*).[32–34] Total weight loss of the GO was about 62.8%. Compared to GO, NGs were quite stable at low temperature region (100–300 °C), indicating the removal of the unstable oxygen-containing functional groups on the surface of graphene during the preparation process. The nitrogen-containing functional groups began to decompose when the temperature went above 400 °C.[26] The TGA results confirmed that the nitrogen-doped graphene had an excellent thermal stability. The total weight loss of NG1, NG2, NG3 was 26.2%, 31.9% and 55.4%. The stability of NGs decreased with the increase of pH values in the reaction environment.

3.3 XPS

XPS was used to characterize composition of the samples as well as the bonding states. Fig. 3(a) shows the XPS survey spectra of NGs. The peaks at 285 eV, 400 eV and 531 eV corresponded to the characteristic peaks of C 1s, N 1s and O 1s, respectively. The existence of N 1s indicates successful nitrogen doping in NGs during the reduction process, of which the residual oxygen content is all above 10%. When the pH value of the reaction environment became larger, the sample NG3 contained more oxygen atoms, resulting from the inhibition of H^+-catalyzed dehydration of oxygen containing functional groups in strong alkaline environment.[35] A small and sharp peak at around 497.4 eV was detected in the XPS survey spectra of NGL-13.9, which is recognized as Na KLL Auger line contributing by the employment of large amount of NaOH.

Further analysis on the high resolution C 1s peaks revealed that the NGs samples contain C–C bonds (sp^2 carbon, 284.5 eV), hydroxyl groups (C–OH, 285.8 eV), epoxy groups (C–O–C, 286.4 eV), carbonyl groups (C=O, 287.1 eV) and carboxyl groups (COOH, 289.2 eV in C 1s), similar to those reported in the literature.[36–38] The contributions of oxygen-containing functional groups obtained by fitting the C 1s spectra for NGs are also listed in Fig. 3(c)–(e). Among all the three types of oxygen functionalities, C=O is considered to provide reversible pseudocapacitance in supercapacitors.[39] As observed from the C 1s spectra in Fig. 3(c)–(e), the content of C=O increases with the pH value. It is worth noting that sample NG3 possessed the lowest amount of carboxyl groups (even less than half of that in NG2). The lack of electronegativity groups in NG3 weakens the electrostatic repulsion of the graphene sheets and narrows the distance, which ultimately leads to aggregation and coagulation of samples.

The nitrogen content of NG1 and NG2 is almost equal (~8.6 at%), which is much higher than that of NG3, revealing that strong basic environment impedes the doping of nitrogen atoms in carbon skeleton. That is mainly because strong alkaline environment results in the decreased capability of ammonia adsorption onto GO surface, which leads to a low nitrogen content.[20,40] Fig. 3(f)–(h) show high resolution N 1s XPS spectrum of the samples, revealing that four types of the bonding states of nitrogen are identified, which corresponds to pyridine nitrogen (N-6) at 398.5 eV, pyrrole nitrogen (N-5) at 399.8 eV, quaternary or graphitic nitrogen (N-Q) at 401.3 eV, and nitric oxide (N-X) at 404.3 eV, respectively.[25,41] Some previous studies proposed that nitrogen located at the edges of graphene layers, for example, N-6 and N-5, can generate pseudocapacitance effect.[26,41] The quantitative analysis based on high resolution N 1s XPS spectrum indicates that NG2 owns highest amount of N-5 and N-6, which is 88.43% among all the nitrogen atoms. As for N-Q, which is deemed to be beneficial to the electric conductivity of carbon materials,[42] sample NG1 has the largest amount as 1.16 at%, while sample NG3 has the highest contribution as 20.85%.

In this process, $(NH_4)_2HPO_4$ was chose as the doping agent. As a typical amphoteric salt, $(NH_4)_2HPO_4$ has a strong tendency to hydrolysis to produce ammonia, which can replace oxygen-containing species on the carbon to form surface groups such as $–NH_2$, –CN, pyrrolic and quaternary nitrogen.[25,41,43] For comparison, we prepare nitrogen-doped graphene reduced by urea (NG-U), of which the mechanism about nitrogen doping is believed to be same as the above description. The XPS spectrum of NG-U is shown in Fig. S1.† The carbon, nitrogen and oxygen content of NG-U obtained from XPS is 80.0 at%, 11.8 at% and

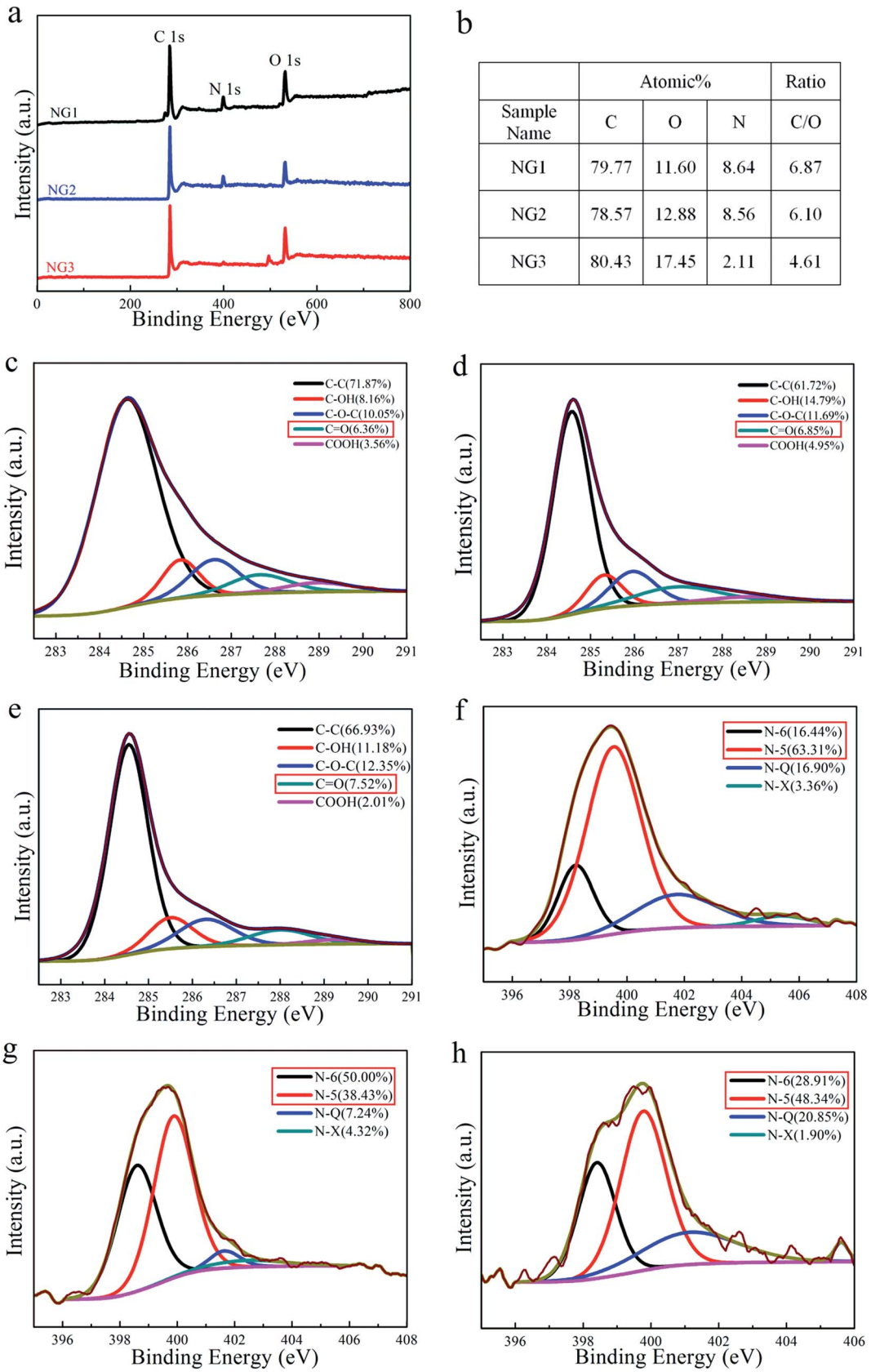

Sample Name	Atomic%			Ratio
	C	O	N	C/O
NG1	79.77	11.60	8.64	6.87
NG2	78.57	12.88	8.56	6.10
NG3	80.43	17.45	2.11	4.61

Fig. 3 (a) XPS surveys of NG1, NG2 and NG3; (b) summary of atomic ratios C/O/N on the basis of the intensities of C 1s, O 1s and N 1s peaks of NG1, NG2 and NG3; the C 1s XPS spectra of (c) NG1, (d) NG2, and (e) NG3; the N 1s XPS spectra of (f) NG1, (g) NG2, and (h) NG3.

8.21 at%, respectively. Compared with NG-U, NGs features less nitrogen atoms and more oxygen atoms, which indicates that using $(NH_4)_2HPO_4$ as doping regent is not as efficient as urea, but results in more oxygen-containing group.

3.4 Electrochemical performance

The electrochemical performance of the prepared samples as electrode materials for supercapacitors was first evaluated through a three-electrode system in alkaline (6 M KOH) electrolytes. Fig. 4(a) shows the CVs recorded using scan rates of 10 mV s^{-1}, exhibiting quasi-rectangular shapes with a pair of faradaic humps. The faradaic humps originate from redox reactions associated with the heteroatoms of N and O, indicating their combined capacitance from the double layer capacitance and pseudo-capacitance in the NGs electrodes.[36] NG2 shows highest pseudo-capacitance than the other two, being evidenced by the apparent oxidation–reduction peaks and largest enclosed area of the NG2 curve, while the shape of CV curve of NG1 almost coincides with that of NG2 except the humps part. The more apparent oxidation–reduction peaks of NG2 can be contributed to its evidently higher amount of C=O and electrochemical active nitrogen-containing groups (N-6, N-5).

Fig. 4(b) shows the GCD curves of NGs at 1 A g^{-1}, demonstrating quasi-linear features due to redox contribution, implying the coexistence of EDLC and pseudocapacitance, which is well consistent with the CV results. The results are similar to those of electrodes based on functionalized graphene materials and reflect the presence of oxygen-containing functionalities and N doping in the NGs electrodes as verified by XPS.[25,44] Corresponding to the CV results, the deviation from linear property in the curve of NG2 is more evident than that of NG1 and NG3, indicating the relative higher contribution of pseudocapacitance from functional groups. As shown in Fig. 4(c), NG2 electrode exhibits highest gravimetric specific capacitance of 399 and 290.8 F g^{-1} at the current densities of 1 A g^{-1} and 20 A g^{-1}, respectively, with retention ratio of 72.88%. NG1 and NG3 show 356, 250 F g^{-1} and 273, 135 F g^{-1} at the current densities of 1 A g^{-1} and 20 A g^{-1}, with retention ratio of 70.22% and 45.45%, respectively. The poorest electrochemical behaviors of NG3 might be mainly related to severe aggregation of graphene sheets which created under strong basic environment, making the electrolyte inaccessible to the large amount of oxygen-containing groups inside. The specific capacitances of NG2 keep higher than those of NG1, which confirms that the presence of oxygen-containing functional groups are more

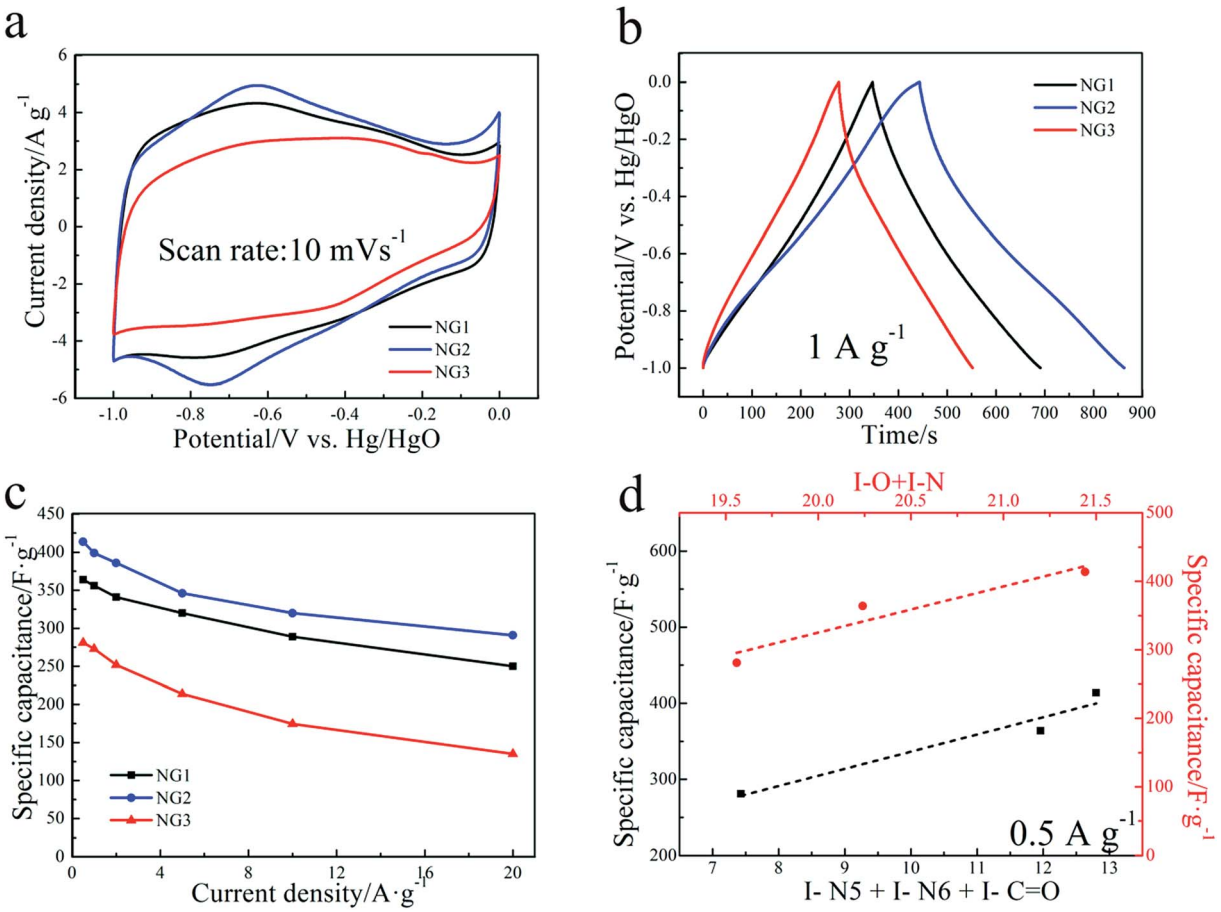

Fig. 4 Electrochemical performance of the samples in three-electrode system. (a) The CV curves of NGs at a scanning rate of 10 mV s^{-1}; (b) the GCD curves of NGs at a current densities of 1 A g^{-1}; (c) the specific capacitance at various current densities of NGs; (d) specific capacitance as a function of the sum of nitrogen and oxygen content (red line) and the sum of I–N5, I–N6, I–C=O content (black line) at 0.5 A g^{-1}.

favorable for the electrochemical energy storage. The highest gravimetric specific capacitances and rate capability of sample NG2 is due to the combination of loose structure (favouring diffusion of electrolyte ion in rapid charge–discharge process) and the pseudo-capacitance from highest content of C=O, N-6 and N-5. For further comparison, the galvanostatic charge/discharge tests of NG-U were also performed as shown in Fig. S2.† With evidently more nitrogen atoms, NG-U exhibits much lower specific capacitance, which is 194.4 F g^{-1} at the current densities of 1 A g^{-1}, even compared with NG3. The low oxygen content of NG-U resulted in its relatively poor capacitance behaviors since certain content of oxygen functional groups contribute to pseudocapacitance as well.[45] The literature related to nitrogen-doped carbon-based materials were shown in the Table S2.†

Nyquist plots (Fig. 5(a)) of the electrodes show that all NGs display small semicircles in the high frequency region and straight lines in the low frequency region. The Nyquist traces were fitted according to an equivalent circuit in the inset of Fig. 5(b), in which R_S is the resistance of the electrolyte; R_{ct} and CPE are the charge-transfer resistance and a constant phase element corresponding to the double-layer capacitance, respectively; Z_w is the Warburg impedance related to the diffusion of electrolyte ions into the bulk electrodes.[30,46] According to the fitting parameters listed in Table 1, the R_{ct} values of NG1. NG2, NG3 are 0.96, 0.68, 0.83 Ω, respectively. The lowest R_{ct} value of NG2 indicates efficient electrochemical processes in the electrode interface.[46] It is known that the Warburg parameter is a decreasing function of ionic conductivity, which indicates the ionic transportation for NGs was promoted with the decrease of pH values. Fig. S4† presents the relationship between the imaginary components of the capacitance (Im(C)) and frequency (log f). The following formula provides such capacitance.[47]

$$C = \frac{1}{j\omega Z} = \frac{1}{j\omega[\mathrm{Re}(Z) + j\mathrm{Im}(Z)]} \quad (1)$$

where Z is the overall impedance of the capacitor cells. This presentation format is advantageous for visualizing the capacitive charging process at low frequencies. The results in Fig. S4† were obtained by incorporating eqn (1) with the impedance data in Fig. 5(a). The imaginary plot of the capacitive response makes it possible to estimate the average relaxation time for charge storage in the electrode: $\tau_0 = 1/f_0$, where f_0 is the peak frequency.[47] As can be seen in Fig. S4,† the f_0 for NG1 and NG2 are almost equal, which is obviously higher than that for NG3. It illustrates the shorter relaxation time for NG1 and NG2, which should be attributed to the increased electronic percolation and ionic transportation caused by their loose structure.

Table 1 Fitting parameters of the Nyquist plots for NGs electrodes

Sample	R_S	R_{ct}	W	CPE
NG1	0.53	0.960	1.77	0.00147
NG2	1.43	0.684	3.83	0.00851
NG3	1.12	0.832	6.54	0.00249

To further understand the combined effect of heteroatoms on the capacitive performance, the relationship between the specific capacitance and the sum of nitrogen and oxygen content is presented (the red line in Fig. 4(d)). The capacitance almost increased linearly with the increase of N and O content confirming the pseudo-capacitance due to synergistic effect of both nitrogen and oxygen functionalities. In order to analyze the electrochemical activity of individual nitrogen/oxygen functionalities, the specific capacitance was analyzed as a function of the combination of pyrrolic nitrogen, pyridinic nitrogen and quinone oxygen (the black line in Fig. 4(d)). These functionalities were selected based on the well-documented case of pseudocapacitance on carbonyl groups[39] as well as proposed faradaic reactions on nitrogen located at the edges of graphene layers, *i.e.*, pyridinic and pyrrolic groups.[41] It is clear that all three functionalities contributed to the pseudocapacitive behavior since capacitance nearly linearly increased with an increase in the total content of the three functionalities, which is also consistent with the results reported by Denisa *et al.*[48]

In order to better study the electrochemical performance of NG2 electrode as a real capacitor in a 6 M KOH solution

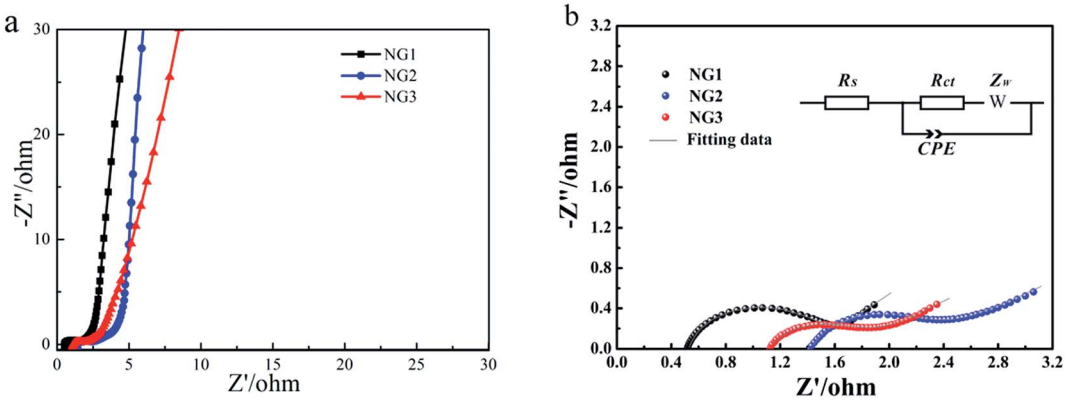

Fig. 5 (a) Nyquist plot of NGs, (b) AC impedance plots and the equivalent circuit for NGs electrodes.

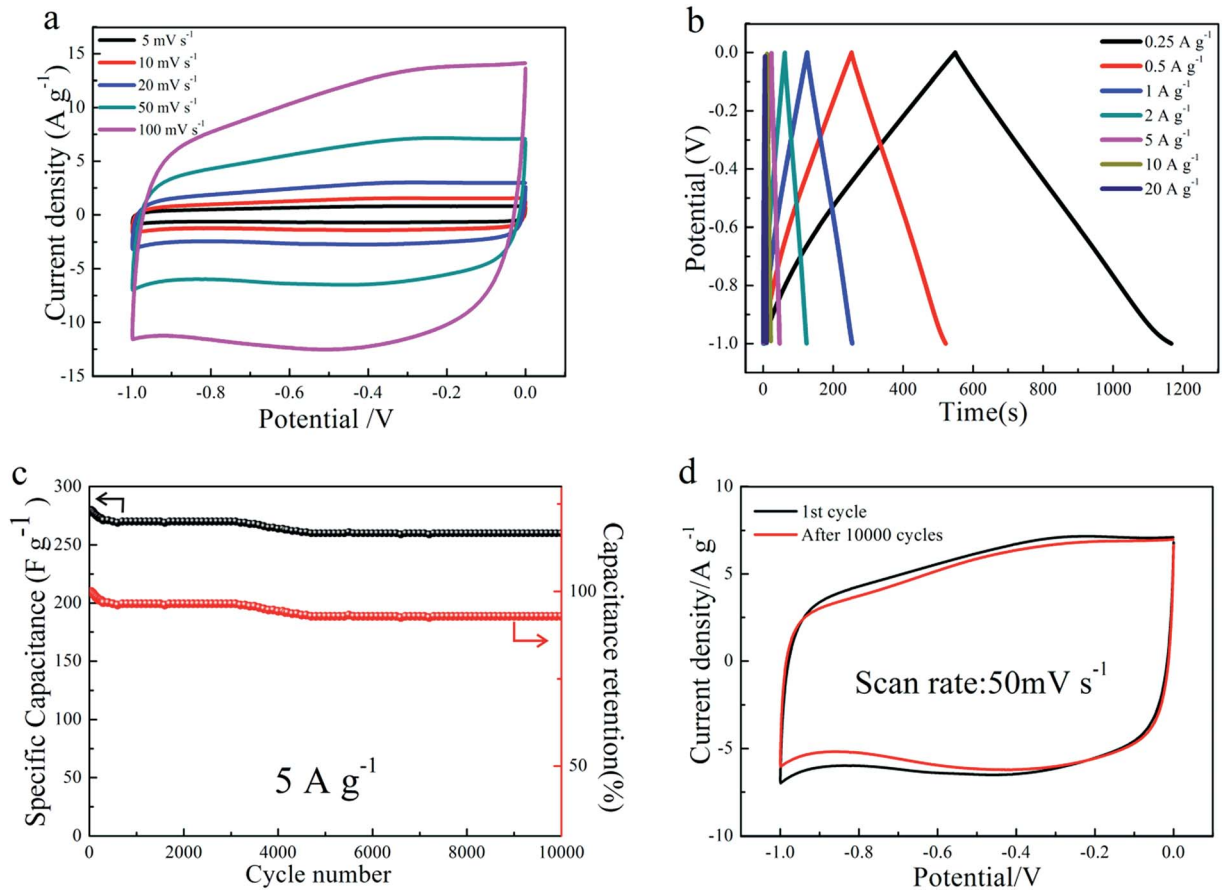

Fig. 6 Electrochemical performance of NG2 in two-electrode system. (a) The CV curves at different scanning rate; (b) the CC curves at various current densities; (c) cycling performance for over 10 000 cycles at 5 A g^{-1}; (d) CV curves of the 1st and 10 000th cycles at a scan rate of 50 mV s^{-1}.

electrolyte, a symmetrical two-electrode configuration was constructed. Fig. 6(a) shows the CV curves of the NG2 electrode at different scan rates (5–100 mV s^{-1}) using a two electrode system. With an increase of the scan rates, the current response increases evidently, without significant changes in the shape of the CV curve, implying the good rate capacity. Perfect rectangular-shaped cyclic voltammogram was still maintained even at a high potential scan rate of 100 mV s^{-1}, further confirming highly capacitive nature and rapid charge–discharge behavior of the electrode.[49] GCD curves at various current densities (Fig. 6(b)) are nearly linear and symmetrical with slight curvature, indicating good capacitive properties and electrochemical reversibility.[41]

The cycling stability of NG2 is evaluated at a current density of 5 A g^{-1} between −1 and 0 V in two-electrode configuration. After 10 000 cycles, the specific capacitance of NG2 decreased from 280 to 260 F g^{-1}, with a capacitance retention ratio of 92.86% (Fig. 6(c)), which hold at 260 F g^{-1} after 5000 cycles, indicative of good long-term cycling durability. The cycling durability of NG2 can be confirmed by the integral areas surrounded by the CV curves of the 1st and 10 000th cycles at a scan rate of 50 mV s^{-1}, as depicted in Fig. 6(d). The decrease of the specific capacitance may be due to the quasireversible or irreversible reaction of electrochemical active functional groups (such as carboxyl and hydroxyl groups).[27]

4. Conclusion

A facile and eco-friendly process has been developed for the production of NG sheets with high nitrogen level *via* the hydrothermal reaction of GO with $(NH_4)_2HPO_4$, in which the resultant supercapacitor performance can be enhanced through simply controlling pH conditions. Weak basic reaction environment endows the electrode with highest specific capacitance (399 F g^{-1} at the current densities of 1 A g^{-1}), best rate capability (72.88% capacitance retention at 20 A g^{-1}) and excellent cyclability (92.86% of the initial capacitance after 10 000 cycles). The outstanding performance can be ascribed to the loosely stacked structure, high content of residual oxygen content, which promises high pseudocapacitance, low-resistant pathways and rapid transport of electrolyte ions, respectively. Therefore, the method employed in this study may provide a way for tuning and optimizing graphene-based supercapacitors beyond their current level of performance.

Acknowledgements

This project is supported by National Basic Research Program of China (973 Program, Grant No. 2014CB660815), the National Natural Science Foundation of China (Grant No. 41202022, 21303129, 51372063), the Fundamental Research Funds for National University (CUG150413, 130403, 1410491B03) China University of Geosciences (Wuhan), and Anhui International Cooperation Project (Grant No. 1303063014). A collaborative project from Guangdong Provincial Key Laboratory of Mineral Physics and Materials (No. GLMPM-003).

References

1 N. G. Sahoo, Y. Z. Pan, L. Li and S. H. Chan, *Adv. Mater.*, 2012, **24**, 4203–4210.
2 L. M. Dai, D. W. Chang, J. B. Baek and W. Lu, *Small*, 2012, **8**, 1130–1166.
3 L. Zhao, L. Z. Fan, M. Q. Zhou, H. Guan, S. Y. Qiao, M. Antonietti and M. M. Titirici, *Adv. Mater.*, 2010, **22**, 5202–5206.
4 L. L. Zhang, R. Zhou and X. S. Zhao, *J. Mater. Chem.*, 2010, **20**, 5983–5992.
5 Y. Sun, Q. Wu and G. Shi, *Energy Environ. Sci.*, 2011, **4**, 1113–1132.
6 T. Kuila, A. K. Mishra, P. Khanra, N. H. Kim and J. H. Lee, *Nanoscale*, 2013, **5**, 52–71.
7 J. L. Xia, F. Chen, J. H. Li and N. J. Tao, *Nat. Nanotechnol.*, 2009, **4**, 505–509.
8 C. Liu, Z. Yu, D. Neff, A. Zhamu and B. Z. Jang, *Nano Lett.*, 2010, **10**, 4863–4868.
9 M. D. Stoller, S. Park, Y. Zhu, J. An and R. S. Ruoff, *Nano Lett.*, 2008, **8**, 3498–3502.
10 Y. W. Zhu, S. Murali, W. W. Cai, X. S. Li, J. W. Suk, J. R. Potts and R. S. Ruoff, *Adv. Mater.*, 2010, **22**, 3906–3924.
11 H. Wang, T. Maiyalagan and X. Wang, *ACS Catal.*, 2012, **2**, 781–794.
12 J. Han, L. L. Zhang, S. Lee, J. Oh, K. S. Lee, J. R. Potts, J. Ji, X. Zhao, R. S. Ruoff and S. Park, *ACS Nano*, 2013, **7**, 19–26.
13 C. O. Ania, V. Khomenko, E. Raymundo-Piñero, J. B. Parra and F. Béguin, *Adv. Funct. Mater.*, 2007, **17**, 1828–1836.
14 L. S. Zhang, X. Q. Liang, W. G. Song and Z. Y. Wu, *Phys. Chem. Chem. Phys.*, 2010, **12**, 12055–12059.
15 H. M. Jeong, J. W. Lee, W. H. Shin, Y. J. Choi, H. J. Shin, J. K. Kang and J. W. Choi, *Nano Lett.*, 2011, **11**, 2472–2477.
16 S. Maldonado and K. J. Stevenson, *J. Phys. Chem. B*, 2005, **109**, 4707–4716.
17 N. Li, Z. Wang, K. Zhao, Z. Shi, Z. Gu and S. Xu, *Carbon*, 2010, **48**, 255–259.
18 D. Long, W. Li, L. Ling, J. Miyawaki, I. Mochida and S. H. Yoon, *Langmuir*, 2010, **26**, 16096–16102.
19 Z. Lei, L. Lu and X. S. Zhao, *Energy Environ. Sci.*, 2012, **5**, 6391–6399.
20 L. Lai, L. Chen, D. Zhan, L. Sun, J. Liu, S. H. Lim, C. K. Poh, Z. Shen and J. Lin, *Carbon*, 2011, **49**, 3250–3257.
21 Y. Chen, B. Q. Xie, Y. T. Ren, M. Y. Yu, Y. Qu, T. Xie, Y. Zhang and Y. C. Wu, *Nanoscale Res. Lett.*, 2014, **9**, 1–8.
22 D. Cai, S. Wang, P. Lian, X. Zhu, D. Li, W. Yang and H. Wang, *Electrochim. Acta*, 2013, **90**, 492–497.
23 T. Wang, L. Wang, D. Wu, W. Xia, H. Zhao and D. Jia, *J. Mater. Chem. A*, 2014, **2**, 8352.
24 B. Q. Xie, Y. Chen, M. Y. Yu, X. Shen, H. W. Lei, T. Xie, Y. Zhang and Y. C. Wu, *Nanoscale Res. Lett.*, 2015, **10**, 1031.
25 L. Sun, L. Wang, C. Tian, T. Tan, Y. Xie, K. Shi, M. Li and H. Fu, *RSC Adv.*, 2012, **2**, 4498–4506.
26 H. Zhang, T. Kuila, N. H. Kim, D. S. Yu and J. H. Lee, *Carbon*, 2014, **69**, 66–78.
27 Y. Fang, B. Luo, Y. Y. Jia, X. L. Li, B. Wang, Q. Song, F. Y. Kang and L. J. Zhi, *Adv. Mater.*, 2012, **24**, 6348–6355.
28 D. Li, M. B. Muller, S. Gilje, R. B. Kaner and G. G. Wallace, *Nat. Nanotechnol.*, 2008, **3**, 101–105.
29 C. Ma, Z. Chen, M. Fang and H. Lu, *J. Nanopart. Res.*, 2012, **14**, 996.
30 D. B. Xiong, X. F. Li, H. Shan, B. Yan, L. T. Dong, Y. Cao and D. J. Li, *J. Mater. Chem. A*, 2015, **3**, 11376–11386.
31 V. B. Parambhath, R. Nagar and S. Ramaprabhu, *Langmuir*, 2012, **28**, 7826–7833.
32 S. Bose, T. Kuila, M. E. Uddin, N. H. Kim, A. K. T. Lau and J. H. Lee, *Polymer*, 2010, **51**, 5921–5928.
33 T. Jiang, T. Kuila, N. H. Kim, B. C. Ku and J. H. Lee, *Compos. Sci. Technol.*, 2013, **79**, 115–125.
34 D. S. Yu, T. Kuila, N. H. Kim, P. Khanra and J. H. Lee, *Carbon*, 2013, **54**, 310–322.
35 Y. Zhou, Q. Bao, L. A. L. Tang, Y. Zhong and K. P. Loh, *Chem. Mater.*, 2009, **21**, 2950–2956.
36 C. Long, L. Jiang, X. Wu, Y. Jiang, D. Yang, C. Wang, T. Wei and Z. Fan, *Carbon*, 2015, **93**, 412–420.
37 C. Yuan, X. Liu, M. Jia, Z. Luo and J. Yao, *J. Mater. Chem. A*, 2015, **3**, 3409–3415.
38 L. Zhou, H. Cao, S. Zhu, L. Hou and C. Yuan, *Green Chem.*, 2015, **17**, 2373–2382.
39 H. Liu, H. Song, X. Chen, S. Zhang, J. Zhou and Z. Ma, *J. Power Sources*, 2015, **285**, 303–309.
40 M. Seredych and T. J. Bandosz, *J. Phys. Chem. C*, 2007, **111**, 15596–15604.
41 D. Wang, Y. Min, Y. Yu and B. Peng, *J. Colloid Interface Sci.*, 2014, **417**, 270–277.
42 F. B. Su, C. K. Poh, J. S. Chen, G. W. Xu, D. Wang, Q. Li, J. Y. Lin and X. W. Lou, *Energy Environ. Sci.*, 2011, **4**, 717–724.
43 D. Hulicova-Jurcakova, M. Kodama, S. Shiraishi, H. Hatori, Z. H. Zhu and G. Q. Lu, *Adv. Funct. Mater.*, 2009, **19**, 1800–1809.
44 Z. Lin, Y. Liu, Y. Yao, O. J. Hildreth, Z. Li, K. Moon and C. P. Wong, *J. Phys. Chem. C*, 2011, **115**, 7120–7125.
45 B. Xu, S. Yue, Z. Sui, X. Zhang, S. Hou, G. Cao and Y. Yang, *Energy Environ. Sci.*, 2011, **4**, 2826–2830.
46 H. R. Naderi, P. Norouzi, M. R. Ganjali and H. Gholipour-Ranjbar, *Powder Technol.*, 2016, **302**, 298–308.
47 C. W. Huang, C. H. Hsu, P. L. Kuo, C. T. Tsieh and T. Teng, *Carbon*, 2011, **49**, 895–903.
48 D. Hulicova-Jurcakova, M. Seredych, G. Q. Lu and T. J. Bandosz, *Adv. Funct. Mater.*, 2009, **19**, 438–447.
49 Y. Bai, R. B. Rakhi, W. Chen and H. N. Alshareef, *J. Power Sources*, 2013, **233**, 313–319.